ANALYSIS OF PERFORMANCES OF HYPERSPECTRAL LIDAR FOR WATER POLLUTION DIAGNOSTICS

Innokenti Sobolev[1], and Sergey Babichenko[2]

1. Tallinn University of Technology, Department of Computer Control, Tallinn, Estonia; isobolevldi(at)gmail.com
2. LDI Innovation, Tallinn, Estonia; sergey.babichenko(at)ldi-innovation.eu

ABSTRACT

The paper is aimed at the analysis of the performances of hyperspectral lidar for detection and classification of oil pollution in water in comparison with a laser fluorosensor having a few discrete detection channels only. It is demonstrated that hyperspectral laser-induced fluorescence (HLIF) spectra include all relevant spectral information about the target in contrast to discrete detection channel sensor data. In order to extract significant features from HLIF data, a multi-resolutional analysis, namely the discrete wavelet transform (DWT), is applied. The feature extraction is automated using the sparsity-norm optimization method. The resulting features have a clear spectral representation and are used in automatic object classification. The classification results and selectivity are compared with discrete detection channel sensor data on a number of oil pollutants. The results of simulation experiments demonstrate the high value of classification accuracy and the ability to sub-classify similar organic compounds from single groups of objects. A comparison with discrete channel sensor data shows a significant increase in the overall performance of oil pollution detection and classification.

INTRODUCTION

Laser remote sensing based on the method of Laser-Induced Fluorescence (LIF) has been recognised in a wide range of environmental applications (e.g., 1,2,3). This includes daily monitoring in open sea areas and detailed tracking of oil spill displacements in the case of large spillages. New applications such as pipeline integrity monitoring, surveillance of coastal waters, waters near offshore platforms, dams, bays, and ports put the conventional active remote sensing systems into a new framework. Under these conditions a lidar should act as a compact standalone analytical instrument designed for early detection and classification of oil discharges into the environment.

LIF lidars used for remote sensing have mainly been used with discrete channel detectors consisting of a set of photomultiplier tubes producing fixed wavelength spectra. The first instruments, namely laser fluorosensors, were first introduced as airborne lidars for oil film detection (1,2). From that point, the capabilities of airborne laser fluorosensors for the detection and classification of oil films with micrometre thickness has been well demonstrated in numerous experiments. Since 1995, new instruments, the hyperspectral LIF (HLIF) lidars, have been tested in airborne open sea area surveillances (4). A distinct feature of HLIF lidar was the recording of continuous emission spectra of objects at every laser shot. The number of detection wavelengths in HLIF lidars increased forty times (from 10 up to 512) in comparison with the conventional fluorosensor.

The reliability of a lidar as an autonomous device is directly dependent on the quality of discrimination of an oil pollution from the natural environment as well as on the classification of the pollutant type. The main source of fluorescence background in natural waters is dissolved organic matter (DOM) of natural origin. Environmental factors influencing the DOM concentration are seawater salinity, climate, season of the year and others (5). The majority of experiments with laser fluorosensors were conducted in open sea areas and over coastal waters with low DOM concentration ranging from 0.1 to 3 mg/l. The absence of strong natural background produced a good identification and classification accuracy of oil pollution for those instruments (6). A good example of oil classification with fluorosensor can be found in (7). However, regions with high DOM content (up to 60 mg/l) like estuaries, lakes, rivers and wetlands have not been considered. The features of

DOI: 10.12760/01-2013-2-04

lidar operations in waters rich in DOM were first studied using the HLIF shipboard lidar in the Baltic and North Seas regions. It has been demonstrated that hyperspectral detection is required to discriminate oil pollution in a variable and strong natural water background (8).

In this article, we present a simulation of HLIF lidar oil pollution detection performance on various DOM concentrations and compare the results with discrete detection channel data. The detection of oil pollution in the presence of high DOM content is based on a comparison of LIF spectral shapes. Using simulation data we provide the classification results of selected refined and crude oil products using their HLIF spectral features. The discrete wavelet transform (DWT) is applied to extract the relevant information from the HLIF spectra. It significantly reduces the dimensionality of data.

SIMULATION

The simulation is based on numerous real-world experimental data sets obtained with airborne HLIF lidar. Figure 1 (left) shows the selected spectra of oil products measured using a hyperspectral lidar with 308 nm excitation wavelength. The typical DOM spectral shape is provided in Figure 1 (right), the maximum of fluorescence emission is at 430 nm. The selected oil products have noticeable shape differences in comparison with the DOM spectrum. For example, the Calsol spectrum is shifted more to the UV with a maximum at 400 nm. On the contrary, crude oils have fluorescences higher than DOM in the blue-green spectral range from 450 to 550 nm. The fluorescence spectra of DOM and oil products can be discriminated using this information.

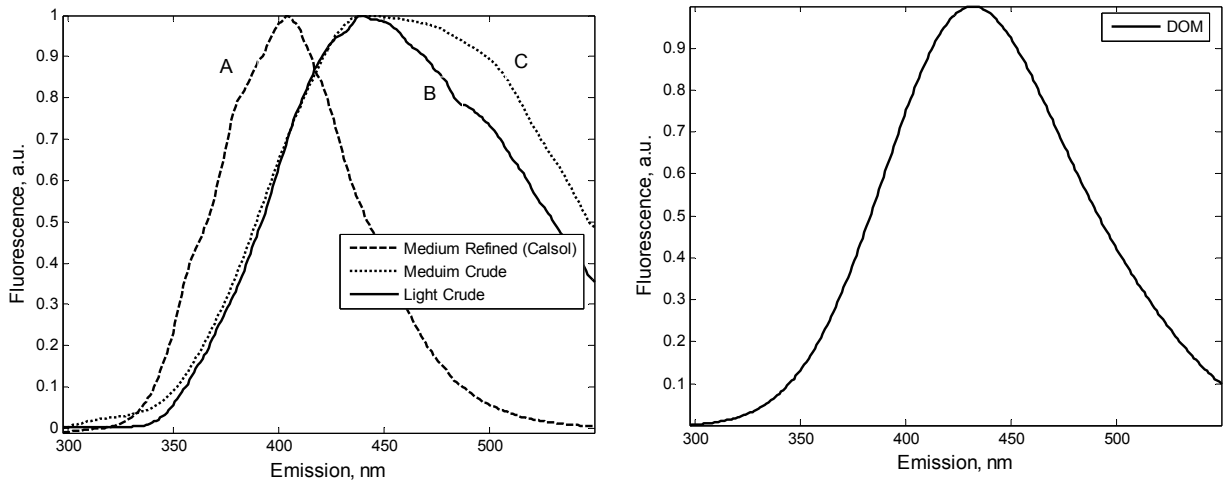

Figure 1 left: The spectra of oil products selected for simulation measured as optically dense thick oil films. Right: The typical shape of a river DOM emission spectrum measured with FLS-AM lidar (8). The water Raman scattering band is removed for better visual spectra comparison. Excitation wavelength is 308 nm.

The simulated HLIF spectra are created as a linear combination of DOM, the water Raman scattering band and one of three selected oil products with an additional noise vector. In the following, the model selection will be explained in more detail. The spectral shapes of a two-component mixture can be treated as a linear superposition of the individual spectral shapes of the component, if no chemical reaction occurs between them, while the intensities of the fluorescence may have a non-linear dependence on the concentrations of individual components due to internal filtering. These non-linearities in the model are not considered in the performance analysis, as they affect the oil fluorescence intensity equally in both the HLIF and discrete channel data. The concentration of oil pollution is selected to be constant at 3 mg/l, which corresponds approximately to a 3 µm oil film on 1 m^2 of water. The DOM concentration is varied in the simulation from 1 up to 40 mg/l, which corresponds to open sea and river water, respectively (9). The fluorescence intensities of DOM and oil pollution in clear water are shown in Figure 2. The value of water Raman scattering is selected to be 200 units, which is typical of open sea water spectra usually recorded with the simulated HLIF lidar at a flight altitude of 200 metres.

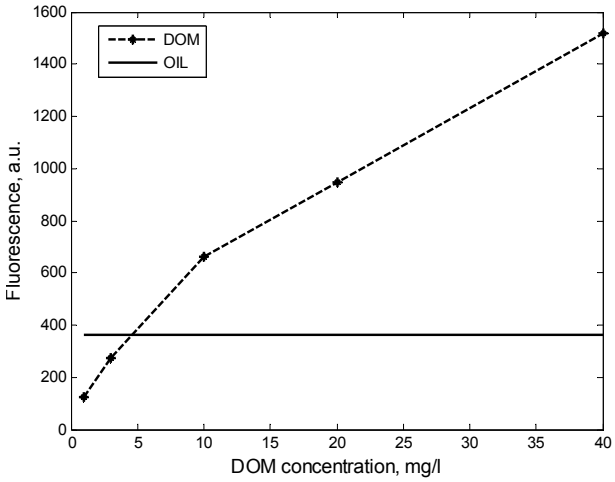

Figure 2: The calibration for DOM and fluorescence intensity of 3 ppm oil in clean water. The DOM concentration values are: 1, 3, 10, 20 and 40 mg/l. Values are estimated using data from (9).

The noise of the FLS-AM lidar data is considered to be shot noise where the signal-to-noise ratio is equal to the square root of the fluorescence intensity. This noise consideration is given by the lidar detector construction based on a gated image intensifier CCD camera. The spectral intensities are expressed in arbitrary units (a.u.) typical of the referenced HLIF lidar. Signal-to-noise (SNR) values of the hyperspectral FLS-AM airborne lidar range from 10 to 20 in single shot measurements.

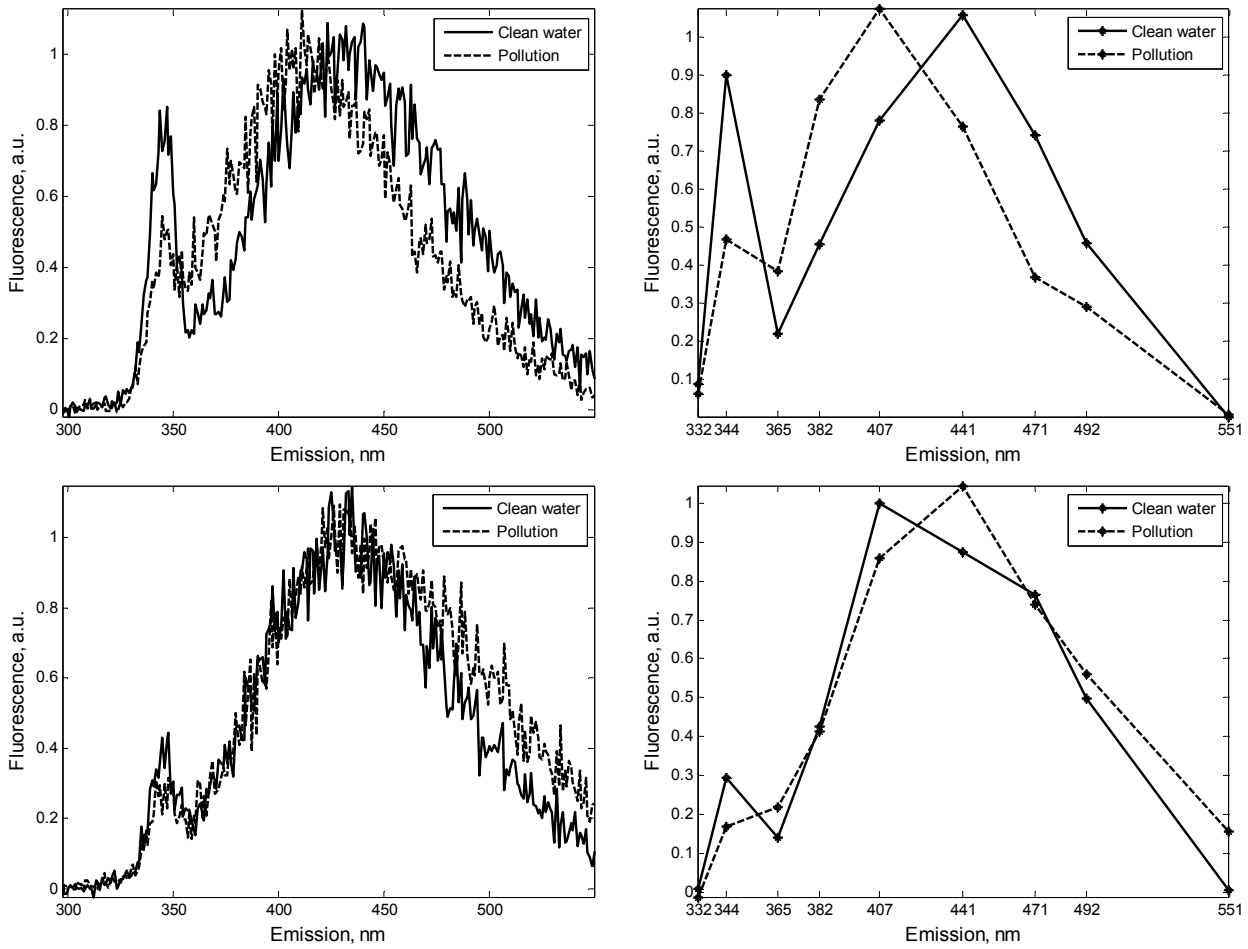

Figure 3: Simulated HLIF spectra (left) and discrete channels (right). Pollution is simulated using Calsol (top) and medium crude (bottom) oils. The DOM concentrations are 3 mg/l and 10 mg/l, respectively.

Simulated laser fluorosensor data are directly derived from HLIF spectra. We selected a typical configuration of discrete emission channels with PMTs and ideal interference filters having a rectangular transfer function, and applied this configuration to HLIF spectra. The selected discrete channels are: 332, 344, 365, 382, 407, 441, 471, 492, and 551 nm, which include the Raman scattering wavelength at 344 nm with 308 nm excitation. The total number of channels is 9 and the optical bandwidth is 10 nm. Modeling a discrete channel with 10 nm spectral width was done by integrating HLIF signals over 20 pixels (0.5 nm each) of the CCD detector. It leads to a 4-5fold increase of the SNR value for the discrete channel detection system. Thus, the effect of bandwidth difference has been properly taken into account. The resulting spectra of HLIF lidar and fluorosensor are shown in Figure 3.

METHODS

Pollution detection

In order to detect contaminants in water with high DOM content a model of the spectral response of a clean water matrix is needed. The water matrix model is created using two vectors, one for the water Raman scattering signal and a second one for DOM fluorescence. Assuming that the LIF spectrum is a linear combination of endmembers, the Raman scattering and DOM intensity in simulated signals $S(\lambda)$ where λ is the wavelength are estimated using the traditional linear spectral unmixing (LSU) method (regression analysis). In vector form the LSU equation can be expressed as:

$$S(\lambda) = \sum_{i}^{n} a_i F(\lambda)_i + e(\lambda), \quad (i = 1,\ 2,\ ...,\ m) \tag{1}$$

where F_i are endmember vectors entering the model, a_i is the intensity value of endmember i and $e(\lambda)$ is the error. Since the intensity a_i of the fluorescence is non-negative we find the solution to (1) using the non-negative least squares algorithm (NNLS). After the estimation of a_i the model of clean water is compared with the simulation spectrum using the coefficient of determination R^2, which is the statistical measure of similarity between the model function and the data. The binary classifier using the threshold $\delta \in (0,1)$ is applied to discriminate between clean and contaminated water spectra. The quality of pollution detection with HLIF and fluorosensor data is evaluated for every DOM concentration using the receiver operating characteristic (ROC) metrics. The ROC metric shows a performance of a binary classifier as its discrimination threshold is varied (10).

Pollution identification

The next operational step is the identification of the pollutant type. This requires the additional sample of the pollutant to be added to the regression model. The estimated coefficients a_i include the intensities of all three endmember vectors (water Raman scattering, DOM and pollutant). The resulting pollutant spectrum is obtained by subtracting the estimated water matrix from the complete signal. Finally, the resulting spectrum is compared with known oil products from the spectral library.

Following the linear spectral unmixing, the comparison of the residual is complicated by the increased relative noise. Indeed, the intensity of the pollutant is only a part of the intensity of the complete signal and thus a linearly extracted pollutant has the same deviation as an unknown noise component in relation to the smaller signal value (Figure 4). This effect is amplified with increasing DOM content in presence of a constant pollution concentration. Thus, high DOM values in water require an additional analysis step to improve the selectivity and quality of the analysis of LIF spectra.

Discrete wavelet-based feature extraction

The wavelet transform (WT) is the most widely used time-frequency analysis of signals in many engineering and scientific applications. A WT is a mathematical representation of arbitrary functions using orthonormal series of wavelet coefficients. The wavelet coefficients represent a time-localised frequency-scale information. Coefficients can be generated using three schemes: con-

tinuous, dyadic and lifting. In this article, a dyadic discrete WT has been applied that produces an optimal representation of signals on a wavelet basis. The dyadic grid allows us to use a fast algorithm, an analogue to FFT, to calculate the WT for discrete sampled data. A formal description of WT is given in (11,12).

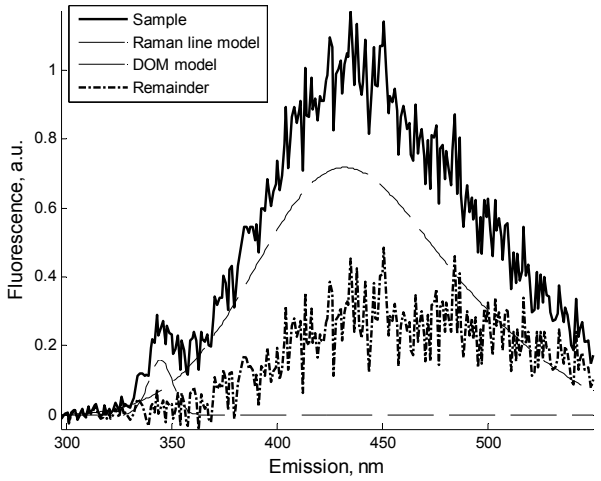

Figure 4: Example of a linear extraction of a pollutant from the simulation sample. The pollutant is Medium crude oil, the DOM concentration is 20 mg/l. The SNR value of the complete spectrum is 13 (set for experiment). The residual intensity is approximately five times lower and thus the residual SNR.

In the case of hyperspectral LIF data, one can extract the significant part and remove the redundant and noisy parts from a spectrum using the WT. The wavelet analysis has the ability to separate the small-scale and large-scale information in high-dimensional data. A good example of the dyadic discrete wavelet transform feature extraction method applied to hyperspectral synthetic aperture radar data is presented in (13). The feature extraction technique proposed in (12) is based on the evaluation of the class-discriminating capability using different subsets of wavelet coefficients and on the determination of a preferably small optimum subset of wavelet coefficients.

In our previous work we proposed a continuous wavelet feature extraction method for HLIF data processing (14). The continuous wavelet transform (CWT) is a redundant and computationally expensive method; however, it preserves the initial spectral information best and excellently extracts all data features. In the CWT feature extraction, the representative scales are individually selected for each pollution type depending on its spectral properties and all coefficients on the selected scales participate in the class comparison. The relation of classification features to spectral properties, like local extreme points, is very important. For example, in Polycyclic Aromatic Hydrocarbons (PAHs), identical local fluorescence extrema areas yield a closely related layout of polyaromatic hydrocarbons and a similar surrounding matrix for complexes of PAHs. The application specific feature extraction method should count the class-discriminating capabilities of features as well as application-specific feature requirements. The latter can be used as an additional constraint of the feature extraction algorithm, as, for example, good features in terms of class-discriminating capabilities can be affected by noise.

In this paper, the DWT version is proposed that uses the main criteria for feature extraction: extracted and selected features are bound to significant spectral properties of the object. The provided feature extraction algorithm exploits the idea of sparsity-norm optimization or basis-pursuit method (15). The signal *s* can be represented using the basis of many functions Φ by minimizing the functional:

$$\left\| s - \tilde{s} \right\|_{l_2} + \lambda \cdot \left\| \alpha \right\|_{l_1}, \quad \tilde{s} = \Phi \alpha \tag{2}$$

where α are the basis coefficients and $\left\| s - \tilde{s} \right\|_{l_2}$ is a reconstruction error. The l_1 norm for α is selected to preserve the sparsity (14). In our approach, the minimization of Eq. (2) must be addition-

ally constrained by the spectral properties of the object. Instead, we use a simplified application-specific algorithm to automatically extract most significant and noise-immune features from the HLIF spectrum.

Since the model spectrum from the spectral catalogue is known to be noiseless, most of the "energy" is allocated between the significant local spectral properties (hills, bends, curves etc.) thus producing the highest corresponding detail coefficients in wavelet decomposition. An optimal and sparse representation of the model is obtained in the following way. In a first step, the complete DWT representation of the model is created on the maximum level of decomposition *M*. Next, the spectrum is reconstructed using only the approximation coefficients $A_m,\ m = M$. In the following steps, the detail coefficients from all decomposition levels $D_m,\ m = 1,2,...,M$, sorted in descending order by their intensity values, are sequentially added to the reconstruction and results are compared with the initial model. Subsequently, the minimum of the sparsity-norm functional is found by comparing the amount of non-zero detail coefficients with the reconstruction quality, Eq. (2). In this experiment, we apply an error threshold of 10% for the reconstruction quality. As the highest detail coefficients are added first, the applied error threshold is reached with the minimal subset of most significant spectral properties.

The feature extraction method is applied to the model of each pollutant and extracted coefficients are stored in a database. The pollutant is identified by computing the probability of a spectrum *i* to belong to the class *j* using the extracted feature values of a model and analysed spectrum:

$$p_{ij} = 1 - \frac{d_{ij}}{d_{\max}} \tag{3}$$

where d_{ij} is an Euclidean distance between the objects *i* and *j*, and $d_{\max}$ denotes the distance from the most distant class for *i*. For discrete channel data, the similarity, Eq. (3), is evaluated directly using the fluorescence values.

RESULTS

Pollution detection

The sets of LIF spectra of clean and polluted water were simulated for each type of pollutant using the method and parameters described above. The simulated discrete channel data from a laser fluorosensor is shown in Figure 5 (left column). In case of DOM concentrations less than 3 mg/l, which correspond mainly to open sea areas, the ROC plot has a point in the upper left corner (coordinate (0,1)), representing perfect classification (no false positives and no false negatives). For high DOM content (10, 20 and 40 mg/l), the detection accuracy degrades, the false positive rate grows and the ROC curve converges to a diagonal line, which means a more random guess of a classifier. The results indicate the expected degradation of detection quality for discrete channel data in waters with high DOM concentrations.

The pollution detection based on fluorosensor simulated data is also affected by the type of oil product. The medium refined Calsol is characterised by a high fluorescence shifted to UV wavelengths and by a narrow spectrum in comparison with the DOM spectrum, which produces a high deformation of the spectral shape (see Figure 3, top). The spectra of crude oils and DOM are broad and mostly overlapped and their linear superposition produces indistinguishable shape variations that are comparable with distortions caused by the detection noise (see Figure 3, bottom). This effect is best seen by comparing the 20 mg/l ROC curves in Figure 5 (left).

The HLIF data (Figure 5, right column) is more sensitive to variations of spectral shape and according to ROC curves the pollution detection results are almost perfect. The negative effect of shot noise is suppressed due to the greatly increased amount of spectral channels. The appearance of pollution adds a large-scale distortion to the spectrum that affects the similarity value more than the small-scale noise distortions. The type of oil still has an effect on the detection quality, which is seen for Light crude oil in Figure 5 (bottom right).

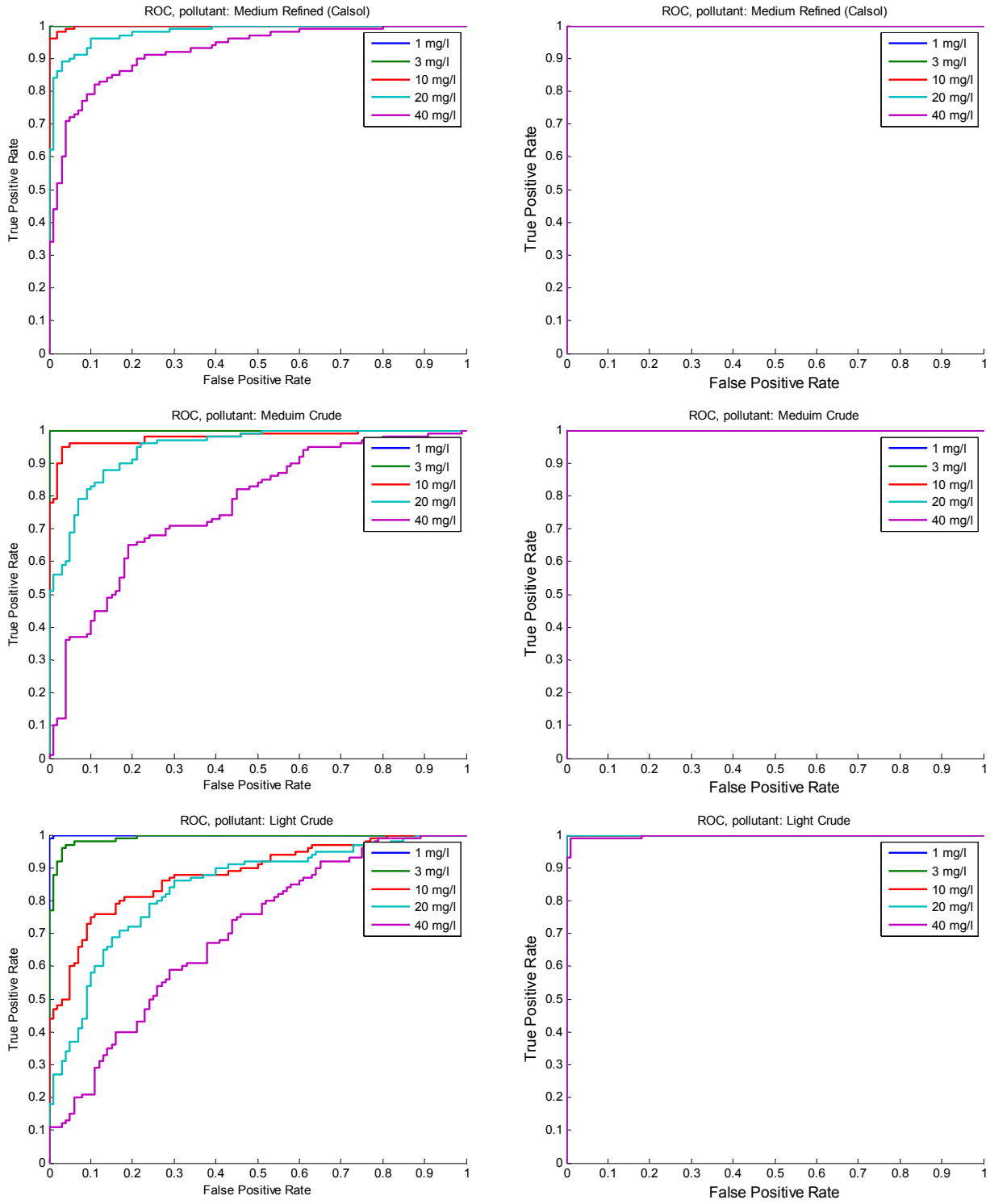

Figure 5: Pollution detection results for fluorosensor (left column) and HLIF (right column) data. The ROC curves are plotted in different colours for DOM concentrations from smallest 1 mg/l (blue) to highest 40 mg/l (violet).

Pollution identification

The pollution identification process is the following step in the operation mode of a lidar. In a real instrument, the identification process relies on the previous step of rough pollution detection. However, here we ignore the non-compliant detection results for fluorosensor data because of high DOM content and assume the presence of a pollution to be known beforehand.

As already stated, the feature extraction represents the first step in the pollution identification process. The model spectra of oil pollution (see Figure 1, left) were analysed using the discrete wavelet-based feature extraction algorithm and results are given in Table 1. The reconstructed versions of model spectra are plotted in Figure 6. The reconstruction error or MSE for all models is less than or equal to 10%.

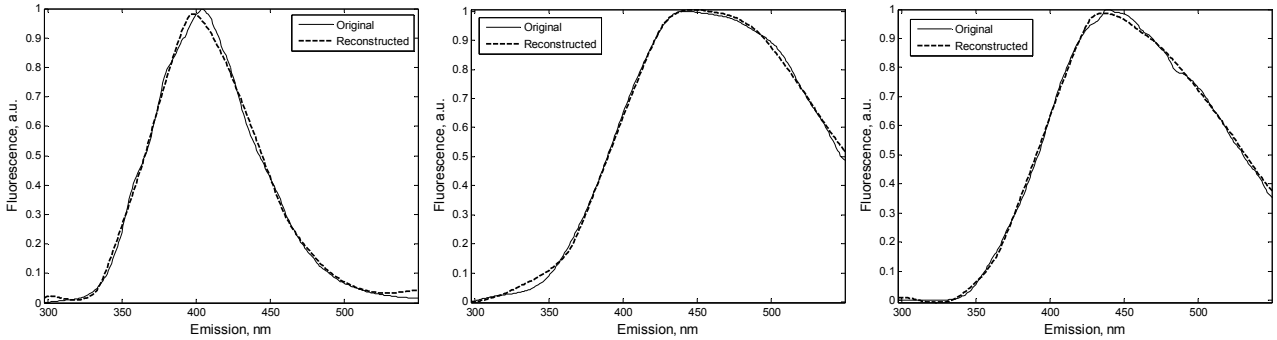

Figure 6: Medium refined (left), Medium crude (middle) and Light crude (right) oil spectra and their reconstruction using the optimal subset of extracted features.

Table 1: Feature extraction results for HLIF data. The maximum level of decomposition M is 7.

	Number of non-zero approximation coefficients (A_7)	Total number of non-zero detail coefficients (D_m)	Corresponding detail coefficients location (nm)
Medium refined	9	6	297, 332, 364, 400, 459, 491
Medium crude	9	3	297, 364, 491
Light crude	10	5	297, 332, 364, 491, 549

The number of non-zero coefficients from Table 1 is significantly less than the number of spectral channels in original HLIF data and is close to the number of channels in a conventional fluorosensor. In (12) it is pointed that approximation coefficients from DWT can be used to mimic a known spectral sensor if the spectral transfer function of the sensor is known. For example, a rectangular transfer function of interference filters matches with the Haar mother wavelet. In our example, we used a more complex and appropriate mother wavelet function from the biorthogonal wavelet family and extracted the significant and sparse information from hyperspectral data. It can be referred to as software imitation of a novel compressed sensing technique (16,17), as we construct a wavelet-based software spectrometer for each specific spectrum.

The classification results are reported using the statistical accuracy measure (ACC) as a proportion of the true results (true positives with true negatives) to the total number of samples (Table 2).

Table 2: Classification accuracy for HLIF and fluorosensor data versus DOM concentration.

DOM concentration (mg/l)	HLIF data			Fluorosensor data		
	Total ACC (%)	cACC (%)	sACC (%)	Total ACC (%)	cACC (%)	sACC (%)
1	100	100	100	87	100	80
3	98	100	97	80	100	70
10	96	100	94	75	99	62
20	90	100	85	72	99	58
40	84	100	80	71	97	57

The classification is performed with a complete set of extracted features, i.e., approximation and detail coefficients for each DOM concentration level. The ACC value is provided for three cases. The total ACC is the overall performance of samples classified by three classes: Medium Refined, Medium Crude and Light Crude. The cACC and sACC values were used to demonstrate the difference in discrimination between different groups of oil products and a sub-classification of the exact oil product. The cACC is the accuracy of classification between the Refined and Crude oil groups. The sACC is the accuracy of sub-classification between Medium and Light crude oils.

In both methods the accuracy of classification between Medium Refined and Crude oils cACC is more than 97% for all DOM concentrations. This result was expected, as the Refined and Crude oils have noticeable differences in fluorescence responses which are detectable in the presence of high noise.

As opposed to this, Medium and Light crude oil spectral responses are highly overlapped which produces more difficulties in their discrimination. The increasing DOM concentration affects the SNR value in the residual signal, which in turn degrades the sub-classification accuracy sACC by 20%. The classification of crude oil types is about 25% better using the HLIF data. For DOM concentrations less than 10 mg/l the sub-classification accuracy is more than 90%. This indicates that hyperspectral data holds robust information that can be well extracted with DWT even in the presence of high noise. Comparing the total performance of the HLIF and fluorosensor data classification, it is clear that the HLIF technique with DWT feature extraction method is superior.

CONCLUSION

The performance of hyperspectral lidar for the detection and classification of organic compounds in water was compared with that of a discrete detection channel laser fluorosensor. The results of simulation experiments demonstrate a superior performance of the HLIF technique in primary oil pollution detection and pollution identification. It is important that the performances were compared in the presence of a natural fluorescence background (DOM) with various concentrations from minor 1 mg/l to high 40 mg/l. The experimental datasets were simulated using real-world data from airborne hyperspectral lidar experiments.

The analysis of HLIF data demonstrated perfect detection results for selected pollutants even in the presence of high DOM content. However, the detection performance with discrete channels is significantly affected by the DOM concentration producing almost random results when the ratio of oil to DOM fluorescence intensities is less than 0.5 (the case of 3 mg/l of oil at DOM concentrations above 20 mg/l for the above simulations). The experiments indicate that the fluorosensor detection performance is also affected by the spectral response of the pollutant. Thus, the selected crude oil products in combination with large DOM produce insignificant variations that are undetectable because of noise distortions.

It was found that detailed spectral information can be extracted from HLIF data using the proposed method based on DWT. The feature extraction method satisfies application-specific feature requirements such as sparsity and direct relation with significant local spectral properties of the object. The dimension of the feature subset is 20 times smaller than the initial dimension of hyperspectra data. The latter is essential for classification, as it eliminates the detrimental effects of high dimensionality. Pollution classification is demonstrated with three oil products selected from two distinct groups of oil: Refined and Crude. The classification accuracy for HLIF data is 100% independent of the DOM concentration. Almost the same result, an average of 99% classification accuracy, is achieved for fluorosensor data.

The more complicated task of detailed sub-classification is shown exemplarily for two Crude oil products. In that case, both methods produce results that are strongly dependent on the SNR value. The sub-classification accuracy decreases to 20% with DOM concentrations increasing from 1 mg/l to 40 mg/l. Due to the robust feature extraction, classification of crude oil types is about 25% better using the HLIF as compared to fluorosensor data.

In future research, a larger experimental dataset including light refined, diesel and other groups of oil products will be studied. The final result could be presented as a technical specification for a hyperspectral LIF lidar analytical platform, for example, as the accuracy of detection and classification of various oil products under different environmental conditions for industrial monitoring applications. The performance of HLIF data analysis relies on the extraction of information from spectra, thus, other methods like matching pursuit could be studied for feature extraction.

ACKNOWLEDGEMENT

This publication was supported by the Estonian Doctoral School in Information and Communication Technology and by the ESF grant Nr 8738.

REFERENCES

1 Hoge F E & R N Swift, 1980. Oil film thickness measurement using airborne laser induced Raman backscatter. Applied Optics, 19: 3269-3281

2 Hengstermann T & R Reuter, 1990. Lidar fluorosensing of mineral oil spills on the sea surface. Applied Optics, 29: 3218-3227

3 Dudelzak A E, S- M Babichenko, L V Poryvkina & K U Saar, 1991. Total luminescent spectroscopy for remote laser diagnostics of natural water conditions. Applied Optics, 30, 453-458

4 Babichenko S, J Lapimaa, L Poryvkina & V Varlamov, 1995. On-line fluorescent techniques for diagnostics of water environment. Proceedings of SPIE, 2503: 157-161

5 Thurman E M, 1985. Organic Geochemistry of Natural Waters (Martinus Nijhoff / Dr W Junk Publ., Dordrecht) 497 pp.

6 Reuter R, H Wang, R Willkomm & K Loquay, 1995. A laser fluorosensor for maritime surveillance: Measurement of oil spills. EARSeL Advances In Remote Sensing, 3(3): 152-169

7 Almhdi K M, P Valigi, V Gulbinas, R Westphal & R Reuter, 2007. Classification with Artificial Neural Networks and Support Vector Machines: Application to oil fluorescence spectra. EARSeL eProceedings, 6(2), 115-129

8 Babichenko S, V Alekseyev, J Lapimaa, A Lisin, L Poryvkina, S Shchemelyov, I Sobolev & L Vint, 2010. Airborne surveillance of water basins with hyperspectral FLS-Lidar. Proceedings of SPIE, 7825: Remote Sensing of the Ocean, Sea Ice, and Large Water Regions, 7825 0K

9 Babichenko S, 2001. Spectral Fluorescent Signatures in Diagnostics of Water Environment (Tallinn: Institute of Ecology) 9985-58-208-x., 53, 60 pp.

10 Hanley J A & B J McNeil, 1982. The meaning and use of the area under a receiver operating characteristic (ROC) curve. Radiology, 143(1): 29-36

11 Daubechies I, 1998. Recent Results in Wavelet Applications. Journal of Electronic Imaging, 7(4): 719-724

12 Daubechies I, 1992. Ten Lectures on Wavelets (Society for Industrial and Applied Mathematics (SIAM)) 357 pp.

13 Bruce L M, C H Koger & J Li, 2002. Dimensionality Reduction of Hyperspectral Data Using Discrete Wavelet Transform Feature Extraction. IEEE Transactions on Geoscience and Remote Sensing, 40(10): 2331-2338

14 Sobolev I & S Babichenko, 2013. Application of the Wavelet Transform for feature extraction in the analysis of hyperspectral laser-induced fluorescence data. International Journal of Remote Sensing, 34(29): 7218-7235

15 Chen S S, D L Donoho & M A Saunders, 2001. Atomic decomposition by basis pursuit. SIAM Review, 43(1): 129-159

16 Donoho D L, 2006. Compressed sensing. IEEE Transactions on Information Theory, 52(4): 1289-1306

17 Chang C C & Lee H N, 2008. On the estimation of target spectrum for filter-array based spectrometer. Optics Express, 16(2), 1056-1061